

Circumstellar interaction of the type Ia supernova 2002ic

N.N. Chugai¹, R.A. Chevalier², P. Lundqvist³

¹*Institute of Astronomy, RAS, Pyatnitskaya 48, 109017 Moscow, Russia*

²*Department of Astronomy, University of Virginia, P.O. Box 3818, Charlottesville, VA 22903, USA*

³*Stockholm Observatory, AlbaNova, Department of Astronomy, SE-106 91 Stockholm, Sweden*

8 October 2018

ABSTRACT

We propose a model to account for the bolometric light curve, quasi-continuum and the Ca II emission features of the peculiar type Ia supernova (SN) 2002ic, which exploded in a dense circumstellar envelope. The model suggests that the SN Ia had the maximum possible kinetic energy and that the ejecta expand in an approximately spherically symmetric (possibly clumpy) circumstellar environment. The Ca II and quasi-continuum are emitted by shocked SN ejecta that underwent deformation and fragmentation in the intershock layer. Modeling of the Ca II triplet implies that the contribution of the O I 8446 Å line is about 25% of the 8500 Å feature on day 234, which permits us to recover the flux in the Ca II 8579 Å triplet from the flux of 8500 Å blend reported by Deng et al. (2004). We use the Ca II doublet and triplet fluxes on day 234 to derive the electron temperature (≈ 4400 K) in the Ca II line-emitting zone and the ratio of the total area of dense fragments to the area of the shell, $S/S_0 \sim 10^2$. We argue that Ca II bands and quasi-continuum originate from different zones of the shocked ejecta that reflect the abundance stratification of the supernova.

Key words: stars: mass-loss – supernovae: general – supernovae: individual (SN 2002ic)

1 INTRODUCTION

Recently, strong evidence has been presented that a sub-class of type IIn supernovae (SN) ('n' stands for narrow H α) includes rare SN Ia events exploding in a dense circumstellar medium (CSM) (Hamuy et al. 2003). To date, the new variety comprises three events: SN 2002ic, SN 1997cy and SN 1999E (cf. Deng et al. 2004). Statistical arguments indicate that the new family constitutes less than one percent of all SN Ia (Chugai & Yungelson 2004). All these supernovae remain very luminous after the light curve maximum, which is related to the CS interaction. A light curve model of SN 1997cy suggests that the CS envelope within 3×10^{16} cm contains several solar masses (Chugai & Yungelson 2004).

Two options for the origin of the CSM have been proposed (Hamuy et al. 2003): mass-loss by a supergiant in a binary scenario of SN Ia (Whelan & Iben 1973) or the mass-loss by a single supergiant in the SN 1.5 scenario (Iben & Renzini 1983). The similarity of SN 2002ic events seems to favour the SN 1.5 scenario, with the progenitor mass around $8 M_{\odot}$ (Chugai & Yungelson 2004). The possible scenario of a C/O white dwarf (WD) merging with the CO-core of a supergiant companion (Livio & Riess 2003) faces a serious problem in explaining the short time lag between the ejec-

tion of the common envelope and the explosion (Chugai & Yungelson 2004).

The study of the CS interaction and modeling of the spectra should elucidate the late evolution and the origin of these interesting events. An important recent conclusion is that SN 2002ic interacts with an equatorially concentrated CSM (Deng et al. 2004). This statement is based upon the interpretation that line profiles in SN 2002ic are too broad compared with the predictions of a spherical model. Also, spectropolarimetric observations of SN 2002ic reveal the presence of polarization which is likely to be related to the CSM (Wang et al. 2004). The claimed asymmetry of the CSM may have an important implication for the problem of the evolutionary scenario, because the single and binary scenarios are likely to possess different degrees of symmetry.

The aspherical model predicts variations of the emission line profiles of SN 2002ic-like supernovae viewed from different angles. However, all three known objects (see Deng et al. 2004, their Fig. 1) show similar shapes and widths of spectral features. This fact implies that, despite the detected polarization of the emission from SN 2002ic, the interaction possesses a high degree of sphericity. In view of this, we investigate a spherical model here. We attempt to explain the light curve, the Ca II line profiles and the quasi-continuum of SN 2002ic-like events on the basis of a

circumstellar interaction model. We rely on the spherical approximation, although we allow for local deviations from sphericity (e.g. clumpy structure). We start with the simulation of the CS interaction dynamics and the bolometric light curve of SN 2002ic using the thin shell approximation (Section 2). Although the model is the same as before (Chugai & Yungelson 2004), we include more realistic ejecta abundances, which affects the light curve. We then analyse the line formation in the inhomogeneous intershock layer and propose a simple treatment of this problem (Section 3). Using this approximation we simulate the Ca II line profiles and the quasi-continuum of SN 2002ic with the kinematic parameters of the interaction model. We demonstrate that the spherical model successfully accounts for the basic observational properties of SN 2002ic and discuss implications.

2 CS INTERACTION AND THE LIGHT CURVE

The interaction of a SN Ia with a dense spherical CS envelope and the light curve formation is calculated using the model applied earlier for the analysis of the CS interaction of SN 2002ic (Chugai & Yungelson 2004). We recapitulate the basic assumptions of the model and emphasize some modifications.

2.1 Model

The density distribution in a freely expanding SN Ia ejecta ($v \propto r$) is approximated by the exponential law $\rho \propto \exp(-v/v_0)$ with v_0 determined by the the mass $M = 1.4 M_\odot$ and kinetic energy E . An exponential law better represents the density distribution in SN Ia ejecta than a power law (Dwarkadas & Chevalier 1998). In an attempt to provide the maximum expansion velocity of the interaction shell we consider a SN Ia model with the maximum kinetic energy, corresponding to the detonation model DET1 of Khokhlov et al. (1993): $E = 1.75 \times 10^{51}$ erg with the ^{56}Ni mass of $M_{\text{Ni}} = 0.92 M_\odot$. We do not claim that the DET1 detonation regime actually occurs in SN 2002ic. This model strongly underproduces intermediate mass elements (e.g. Ca) (Khokhlov et al. 1993), which is at odds with the strong Ca II lines observed in SN 2002ic (see below Sec. 3.4). Parameters of the DET1 model are adopted because this case illustrates what happens if all of a Chandrasekhar mass C/O WD is burned. The important point here is that the complete incineration of C and O is not required: if the burning in the outer layers is terminated at the intermediate elements, the released nuclear energy is practically the same as in the case of complete incineration.

The CS density distribution is described by power laws ($\rho \propto r^k$) with different power law indices for each of three suggested radial zones: k_1 in the range $r < r_1$, k_2 for $r_1 < r < r_2$, and k_3 for $r > r_2$. The variation of the power law index is suggested by two observations: (i) the luminosity decline after about day 400 (Deng et al. 2004) suggests a CS density drop beyond some radius $r > r_2$; (ii) the rising early visual luminosity of SN 2002ic (Wood-Vasey et al. 2002; Hamuy et al. 2003) suggests a flat (or rising outwards) CS density distribution in the inner part ($r < r_1$) of the CS envelope (Chugai & Yungelson 2004).

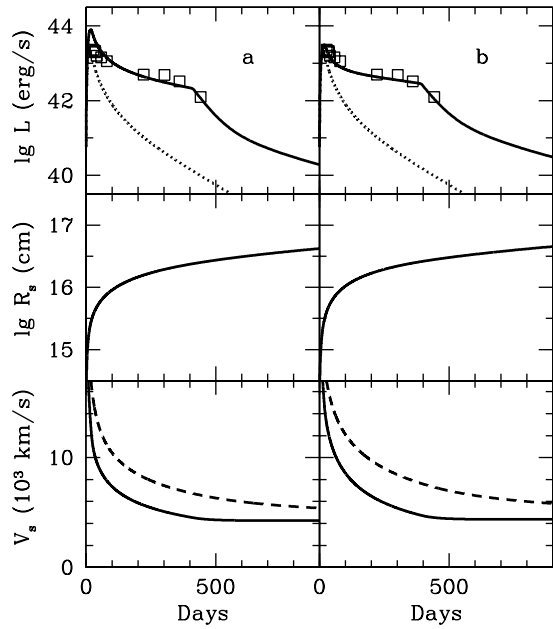


Figure 1. Bolometric light curve (upper panels), radius of the thin shell (middle), and expansion velocity (bottom) for models with CS density $\rho \propto r^{-2}$ (a) and $\rho \propto r^{-1.4}$ (b). The bolometric light curve with CS interaction (solid line) and without CS interaction (dotted) are overplotted on the data of Deng et al. (2004). The lower panel shows the velocity of the thin shell (solid) and the SN boundary velocity (dashed).

The hydrodynamic interaction is calculated in the thin shell approximation, in which the layer between the forward and reverse shocks is replaced by a geometrically thin shell (Chevalier 1982b). The kinetic luminosities of the forward and reverse shock waves are converted into X-ray luminosities using transformation coefficients dependent on cooling rates of the postshock gas and the expansion time (Chugai 1992; Chevalier & Fransson 1994). For the CS density range of interest, the reverse shock is always radiative, which leads to the formation of a cool dense shell (CDS) composed of the shocked SN ejecta. The forward shock can be also radiative and contribute to the CDS formation. The X-ray radiation of both shocks absorbed by the cool material (SN ejecta, CDS, and CSM) is identified with the optical bolometric luminosity powered by the CS interaction. The additional luminosity powered by the radioactive decay $^{56}\text{Ni} - ^{56}\text{Co} - ^{56}\text{Fe}$ is calculated using an analytical theory for the SN light curve (Arnett 1980). The resulting light curve is the sum of the interaction and radioactive luminosities.

An important modification in the present version is the inclusion of a ‘realistic’ chemical composition of the SN Ia ejecta instead of the previously assumed solar composition (Chugai & Yungelson 2004). The SN Ia composition is now approximated by a mixture of Fe and Si, where the amount of Fe is equal to the ejected ^{56}Ni mass. The new composition results in more efficient cooling in the reverse shock and more efficient absorption of the X-rays in the SN ejecta. The adopted absorption coefficient for X-rays in the SN material is $k_X \approx 500 E_{\text{keV}}^{8/3} \text{ cm}^2 \text{ g}^{-1}$, i.e., 50 times larger than that with a solar composition. Owing to the efficient absorption

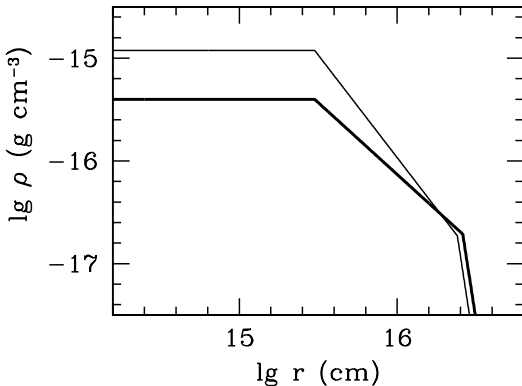


Figure 2. Circumstellar density in the model with $\rho \propto r^{-2}$ (thin line) and $\rho \propto r^{-1.4}$ (thick line). In both models, the inner zone has a plateau density distribution to provide the rise of the light curve to the maximum at about day 20.

of X-rays in the SN Ia ejecta with the ‘realistic’ composition, the rate of emission of optical photons per unit of kinetic luminosity is higher in the present model compared with the earlier version.

2.2 Light curve

Our modeling of the bolometric optical light curve is compared with the SN 2002ic data from Deng et al. (2004), modified here for a Hubble constant of $H_0 = 70 \text{ km s}^{-1} \text{ Mpc}^{-1}$. Two versions of the light curve computations along with the corresponding shell radius and velocity are presented in Fig. 1. Fig. 1a shows the model with $k_2 = -2$, whereas the second model (panel b) corresponds to $k_2 = -1.4$. Both CS density distributions are shown in Fig. 2. The model with $k_2 = -1.4$ provides the largest expansion velocities of the thin shell (v_s) and of the SN at the boundary (v_{sn}). From the point of view of the interpretation of the observed broad line profiles, this model is preferred. Henceforth, this case is referred to as the standard model.

The flatter CS density distribution of the model compared with a steady-state wind implies that after the main mass loss episode, the mass loss rate gradually decreased while the presupernova evolved towards the explosion. The total mass of the CS envelope in the standard model is $1.6 M_{\odot}$. This estimate should be considered a lower limit, because we neglect the possible wind at $r \gg r_2$ that may comprise a significant mass, despite its lower density. If the wind velocity out to $r_2 \approx 2.6 \times 10^{16} \text{ cm}$ is $> 10 \text{ km s}^{-1}$, then the age of the strong mass loss is $< 820 \text{ yr}$ and the mass loss rate is $> 2 \times 10^{-3} M_{\odot} \text{ yr}^{-1}$.

We recalculated the light curve of SN 1997cy for the detonation model with a ‘realistic’ composition and found that the mass of the CS envelope in this case is $\approx 2.5 M_{\odot}$, a factor two lower than our previous estimate for SN 1997cy based upon a model with lower explosion energy and normal composition of the SN ejecta (Chugai & Yungelson 2004). Most of the difference is related to the efficient conversion of the kinetic luminosity into the bolometric luminosity owing to the efficient absorption of X-rays by the ejecta.

The model of the optical light curve predicts the luminosity and flux of the escaping X-rays, which may be used as an additional test of the model for SN 2002ic-like events. In Fig. 3, we plot the total luminosity of the escaping X-rays from the forward and reverse shocks, together with the temperatures of both shocks for the standard model. Due to the high CS density and rather flat CS density distribution, the velocity jump at the inner shock is relatively high (Fig. 1). This, combined with the higher molecular weight of the SN Ia matter, results in a high temperature of the reverse shock that is comparable to the temperature of the forward shock after day 250. In a SN II interacting with a wind, the reverse shock is usually markedly slower and cooler than the forward shock (Chevalier 1982b). Remarkably, the luminosity of the forward shock is large and provides a substantial contribution to the optical SN luminosity. This is due to the fact that the forward shock is radiative: it enters the fully radiative regime on day ~ 150 . The reverse shock is radiative through the time period we have modeled. The inflection in the forward shock luminosity on day ~ 400 reflects the corresponding inflection in the adopted CS density distribution at $r \approx 2.6 \times 10^{16} \text{ cm}$ (Fig. 2). The forward shock becomes nonradiative soon after that point, at $t > 440 \text{ d}$.

The photon spectrum of the emergent X-ray flux at different epochs between day 30 and day 600 is shown in Fig. 4 together with the detection limit of the JEM-X monitor of the INTEGRAL satellite assuming a 3σ detection level with the integration time of 10^6 s (<http://astro.estec.esa.nl/Integral/>). The plot demonstrates that the detection of X-rays from SN 2002ic is not expected in our model for a reasonable integration time. On the other hand, a SN 2002ic-like event exploding at a distance $D \leq 100 \text{ Mpc}$ would be detectable at the favorable epoch of 200–400 days by the JEM-X monitor with an integration time $\leq 10^6 \text{ s}$. Chandra and XMM may be even more efficient in detecting the X-rays from distant SN 2002ic-like events. Between days 200–500 the predicted flux of SN 2002ic in the $0.5–10 \text{ keV}$ band is $\sim 10^{-14} \text{ erg s}^{-1} \text{ cm}^{-2}$. Given the Chandra detection limit $\sim 10^{-15} \text{ erg s}^{-1} \text{ cm}^{-2}$ in the $0.5–10 \text{ keV}$ band, we conclude that X-rays from SN 2002ic could have been detected at an age 200–500 days. At later epochs, the flux quickly decreases (Fig. 4) and on day 600 it becomes far below the Chandra sensitivity.

The above model for the escaping X-ray flux assumes a smooth CSM. Clumpiness may modify these results in two ways: a different temperature in the forward shock, and a different escape probability for photons through the clumpy CSM.

3 FORMATION OF THE OPTICAL SPECTRUM

The late time Subaru spectrum on day 234 (assuming the explosion date JD 2452585) consists of broad emission bumps (we dub them quasi-continuum) with superimposed emission lines of H α , H β , Ca II 3900 Å, and Ca II 8600 Å blended with O I 8446 Å (Deng et al. 2004). Most of the bolometric luminosity in our dynamical model comes from the shocked ejecta. We, therefore, believe that, apart from H α and H β and other narrow lines, most of the optical spectrum on day

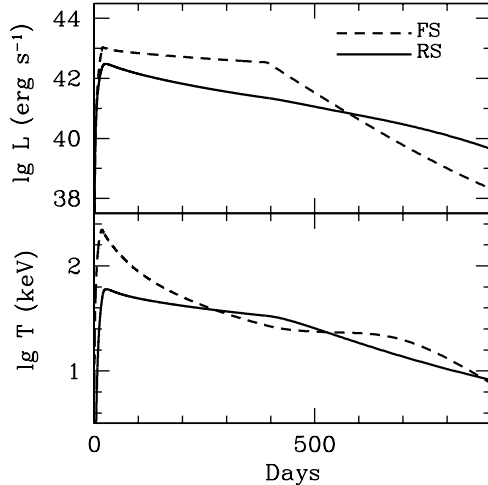


Figure 3. Luminosity of escaping X-rays (top) and temperature (bottom) of the reverse shock (solid line) and forward shock (dashed)

234 (i.e. quasi-continuum and Ca II lines) originates from shocked SN ejecta. This conjecture will be checked below.

We only briefly address the important issue of H α line formation. Although the CS origin of the narrow H α emission is certain, the nature of the broad H α is unclear. Multiple Thomson scattering as a mechanism for the broad H α , applied earlier to SN 1998S (Chugai 2001), and discussed by Wang et al. (2004) in connection with SN 2002ic, requires a large optical depth $\tau_T \sim 3$. This is in conflict with our dynamical model that predicts a Thomson optical depth of the undisturbed CS ejecta of $\tau_T \approx 0.1$ on day ≈ 240 . In our opinion, the broad H α comes from the shocked cool dense hydrogen. There are three possible origins for that line-emitting gas: (i) the outer layers of the SN ejecta may contain the remains of the hydrogen envelope of the presupernova (in the SN 1.5 scenario), so the cool shocked ejecta enriched by hydrogen may be partially responsible for the broad H α component; (ii) the forward shock becomes radiative in the case of smooth CS hydrogen after about day 150, so the shocked CS hydrogen cools at that epoch and becomes able to emit broad H α ; (iii) in the case of a clumpy CS envelope radiative shocks in CS clouds and the shear flow around the shocked clouds may produce the broad velocity spectrum of the line-emitting gas that can be responsible for the intermediate and broad H α line. In reality, all three sources of the cool shocked hydrogen may contribute to the broad H α component. However, only in the third option can the observed intermediate H α component with a width of $\sim 2 \times 10^3$ km s $^{-1}$ (Hamuy et al. 2003) be produced.

Henceforth, we concentrate on the study of the Ca II emission lines and the quasi-continuum.

3.1 Line formation model

Momentum and mass conservation imply a very small thickness of the CDS, of the order of $\delta \sim R(v_{\text{sh}}/c_s)^2$, where $v_{\text{sh}} = v_{\text{sn}} - v_s$ is the velocity of the reverse shock and c_s

is the ion sound speed in the cool gas. With $v_{\text{sh}} \approx 3000$ km s $^{-1}$ at an age of 230-250 d (see Fig. 1), adopting the temperature of the cool gas of 10 4 K and the ion average atomic weight ≈ 40 (i.e., $c_s \approx 2$ km s $^{-1}$), $\delta/R \sim 10^{-6}$. For such a thin shell the velocity dispersion along the line of sight is negligible, so the line radiation transfer in this shell may be treated in the static approximation (Chevalier and Fransson 1994). The expansion effect appears only in the transformation of the shell emission to the observer frame. However, the picture of a spherical thin CDS is an idealization; in reality, as we will show below, the shell should be strongly distorted.

3.1.1 Line-emitting shell

A straightforward argument against the existence of a geometrically thin spherical shell is based upon the observed profiles of the Ca II features. It is well known that in the optically thin case the line profile from a geometrically thin expanding shell should be boxy. This might be a sensible approximation for the observed Ca II features given some unavoidable perturbation and smearing of the boxy profile. The problem, however, is that the Ca II lines are expected to be optically thick, not thin.

To show that the dense shell is opaque in the Ca II lines, we consider the conditions on day 240. The swept up SN mass in the reverse shock in the standard model is $\approx 0.6 M_\odot$ and the shell radius is $R \approx 1.8 \times 10^{16}$ cm. Assuming that the swept up mass resides in the CDS and that the Ca abundance among Fe-peak elements is solar, i.e., ≈ 0.03 by mass (a sensible approximation for a rough estimate) one gets the column density of Ca II in the CDS of $N(\text{CaII}) \sim 2 \times 10^{20} \phi_2$ (where ϕ_2 is the ionization fraction of Ca II). The optical depth in the Ca II doublet lines is then

$$\tau = \frac{\pi e^2}{mc} \frac{f_{12}}{u_t} N(\text{CaII}) \sim 10^9 \phi_2, \quad (1)$$

where $f_{12} = 1$ is the oscillator strength for the Ca II doublet and $u_t \sim 2$ km s $^{-1}$ is the thermal velocity assuming $T = 10^4$ K. On day 234, the number density in the CDS under pressure equilibrium is $\sim 10^{13}$ cm $^{-3}$. Assuming LTE in the cool dense gas we obtain $10^{-3} < \phi_2 < 1$ for $4000 < T < 10^4$ K. The equation (1) shows that the optical depth of the CDS in the Ca II doublet is very large for the estimated Ca II ionization fraction. It is easy to check that, given the low excitation potential of the Ca II term ^2D , the Ca II triplet should be optically thick too.

Optically thick Ca II lines from a geometrically thin shell are expected to be double-horned (M-shaped) $F \propto |\lambda - \lambda_0|$ with peaks at the shell velocity ($\pm v_s$) (Gerasimović 1933). This type of profile is apparently inconsistent with the smooth, round-topped (flat-topped) Ca II doublet and triplet profiles observed in SN 2002ic (see Deng et al. 2004). To resolve this controversy, we follow Cid Fernandes & Terlevich (1994) in suggesting that the round-topped H α line profile observed in SNe II interacting with a dense CS environment are produced by a thin shell corrugated due to the Rayleigh-Taylor (RT) instability.

It is well known that the decelerated thin shell in the intershock layer is subject to the Rayleigh-Taylor (RT) instability (Chevalier 1982a; Nadyozhin 1985). RT spikes grow and degrade via shearing and advective flows, thus produc-

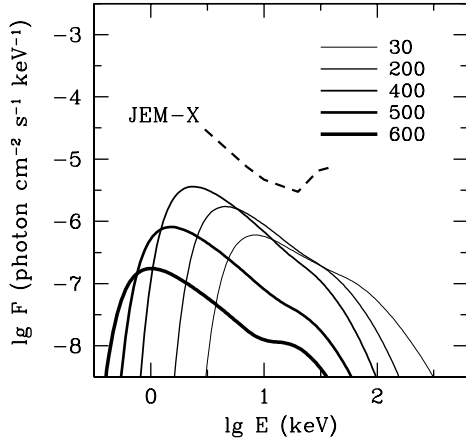


Figure 4. X-ray photon flux from SN 2002ic predicted by the standard model at different epochs between days 30 and 600 assuming $H_0 = 70 \text{ km s}^{-1} \text{ Mpc}^{-1}$ ($D = 285 \text{ Mpc}$). The 3σ sensitivity curve of JEM-X monitor of INTEGRAL (dashed line) assumes a 10^6 s integration time.

ing a two-fluid mixture consisting of dense cool gas and hot postshock gas behind the forward shock wave. As a result, a mixing layer with an extent $\Delta R/R \sim 0.1$ forms between the thin shell and the forward shock as demonstrated by 2D and 3D simulations (Chevalier & Blondin 1995; Blondin & Ellison 2001). The clumpy structure of the CSM may cause additional perturbations of the mixing layer and lead to the corrugation of the forward and reverse shocks (Blondin 2001, his Fig. 6). If both reverse and forward shocks are radiative, the shell instability becomes even more vigorous due to the nonlinear thin shell instability (Blondin & Marks 1996; Hueckstaedt 2003). The above arguments based upon the profile shape and the interaction hydrodynamics suggest that a realistic model of the intershock line-emitting layer should include the inhomogeneous distribution of the dense shocked gas.

To treat the line formation in the inhomogeneous intershock layer, we reduce it to a spherical ‘shell’ of a thickness $\Delta R = 2\xi R = 0.1R$ in the range of radii $|r - R| < \xi R$ filled with similar, randomly oriented, dense planar fragments (Fig. 5). Each fragment is a thin sheet with an area σ and total surface area 2σ . As a result of the deformation and stretching of dense fragments, their cumulative area S should, generally, exceed the area of the unperturbed spherical dense shell $S_0 = 4\pi R^2$ by a factor $S/S_0 > 1$. As we will see below, this parameter (called the ‘area ratio’) turns out to be crucial for the interpretation of the high luminosity of the Ca II features in SN 2002ic. Moreover, the high luminosity of the Ca II features requires $S/S_0 \gg 1$. This is the reason why we omit in our simple model (Fig. 5) the thin spherical shell that is produced and destroyed continuously in the reverse shock.

3.1.2 Line radiation transfer in the shell

We consider two plausible velocity distributions of filaments in the shell $R(1 - \xi) < r < R(1 + \xi)$: a constant velocity and a linear law $v = v_s(r/R)$. Line photons emitted by

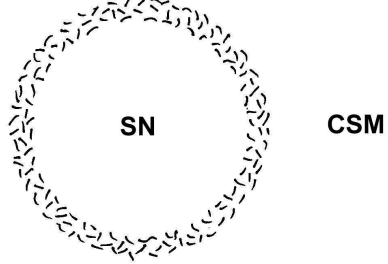


Figure 5. A schematic view of SN 2002ic that shows the fragmented cool dense shell responsible for the bulk of the optical radiation. The fragmented shell is bounded by the forward shock propagating in the CSM and by the reverse shock propagating in the unshocked SN ejecta.

randomly distributed dense fragments may escape or be absorbed by another fragment of the shell. To describe the line radiative transfer inside the inhomogeneous shell we apply the local escape probability language adapted for the ‘gas’ of opaque macroscopic chunks of dense material. Definitions of the local optical depth and emissivity must be modified accordingly.

The total number of fragments in the shell is $N = 4\pi R^2(S/S_0)/\sigma$ and the fragment number density is $n_f = N/V = (S/S_0)/(\sigma\Delta R)$, where $V = 4\pi R^2\Delta R$. The average cross-section of a fragment is $\langle\sigma\rangle$ with the ratio $\langle\sigma\rangle/\sigma = 0.5$ for plane sheets and ~ 0.5 for deformed sheets. For instance, for a cylindrical surface with a radius a and a height $h \ll a$ this ratio is ≈ 0.5 with the accuracy of $O(h/a)$. The radiation escapes from an optically thick fragment in the frequency band $2x\Delta\nu_D$ assuming a gaussian absorption coefficient $k_\nu \propto \exp[-(\Delta\nu/\Delta\nu_D)^2]$, where $\Delta\nu_D = u_t/\lambda$ and x is defined by the condition $\tau(x) = 1$, i.e., $x = (\ln \tau)^{0.5}$. A fragment absorbs the incident radiation in the same frequency band, $2x\Delta\nu_D$.

The analog of the Sobolev optical depth in our case is the local occultation optical depth, $Q = 2xu_t\langle\sigma\rangle n_f |dv/ds|^{-1}$. To take into account the finite optical depth of a fragment this expression should be multiplied by the absorption probability of a fragment $(1 - e^{-\tau})$. For a shell with constant velocity, the velocity gradient along some direction is $dv/ds = (v_s/R)\sin^2\theta$, where θ is the angle between the photon wave vector and the radius. The expression for Q then reads

$$Q = \frac{x}{\sin^2\theta} \left(\frac{S}{S_0} \right) \left(\frac{R}{\Delta R} \right) \left(\frac{u_t}{v_s} \right) (1 - e^{-\tau}) = Q_0(1 - e^{-\tau})/\sin^2\theta, \quad (2)$$

where $\langle\sigma\rangle/\sigma = 0.5$ is used. For the linear velocity case, $Q = Q_0(1 - e^{-\tau})$. To estimate Q_0 let us adopt $v_s = 6000 \text{ km s}^{-1}$, $u_t = 2 \text{ km s}^{-1}$ and $x \approx 3$. Equation (2) gives $Q_0 \sim 10^{-2}(S/S_0)$. Therefore, the shell becomes optically thick ($Q_0 > 1$) for an area ratio $S/S_0 > 10^2$ provided $\tau \gg 1$.

The emissivity of the fragment ensemble is $j = (1/2\pi)\sigma n_f F$, where F is the frequency integrated flux. In the isothermal approximation and assuming Boltzman pop-

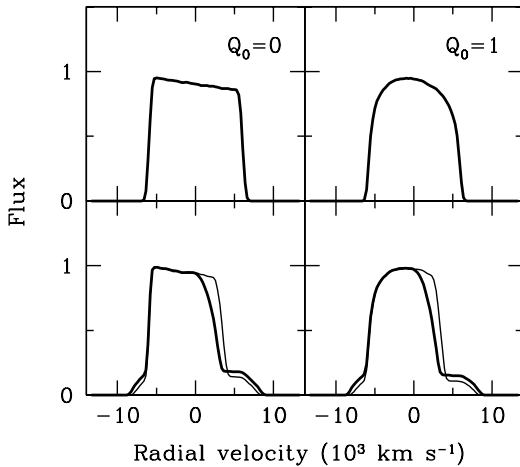


Figure 6. The line profile for two different models of the cold, dense shell. Upper panels show profiles for a transparent ($Q_0 = 0$) and a modestly opaque shell ($Q_0 = 1$). Lower panels show profiles for the same models, but with the addition of non-local scattering in the SN ejecta for a cut-off radius $r_c = 0.95$ (thick line) and $r_c = 0.9$ (thin line).

ulations, the flux is $F = 2\pi B_\nu(T)x\Delta\nu_D(1 - e^{-\tau})$, so the emissivity is

$$j = \sigma n_f B_\nu(T)x\Delta\nu_D(1 - e^{-\tau}). \quad (3)$$

To compute the luminosity, one needs to take into account self-absorption via the angle-averaged escape probability $\beta = \langle [1 - \exp(-Q)]/Q \rangle$. Assuming pure absorption one gets the luminosity $L = 4\pi jV\beta$, where V is the shell volume $4\pi R^2\Delta R$. With the line emissivity j from equation (3), the luminosity of Ca II triplet is

$$L = 16\pi^2 R^2 (S/S_0) B_\nu(T) (1 - e^{-\tau}) \beta x \Delta\nu_D. \quad (4)$$

The luminosity increases linearly with the area ratio for $Q_0 \ll 1$ (i.e., $\beta \approx 1$) and saturates for large S/S_0 , when Q_0 becomes also large. Actually, for large Q_0 one gets $\beta \sim 1/Q_0 \propto S_0/S$ so L becomes independent of S/S_0 . Remarkably, the line luminosity according to equation (4) exceeds the upper limit on the luminosity of a static shell by a factor $(S/S_0)\beta$ that, for large area ratio, may be substantially greater than unity. This apparent paradox is related to the velocity gradient that permits the volume emission regime for resonance photons as opposed to the surface emission regime in the static case. A finite albedo ω of a fragment for incident photons requires a modification of the escape probability: β in equation (4) should be replaced by $p = \beta/[\beta + (1 - \beta)(1 - \omega)]$. However, we compute the line profiles on the assumption of zero albedo, which, as we checked, does not affect the profile significantly.

In the limit of a small area ratio ($S/S_0 \sim 1$) the luminosity of the Ca II triplet on day 234 for the probable temperature range $T < 10^4$ K for $\beta = 1$ is $L(8579\text{\AA}) < 5 \times 10^{40}$ erg s $^{-1}$. On the other hand, using the flux in the 8500 Å band, $f \approx 4.7 \times 10^{-14}$ erg s $^{-1}$ cm $^{-1}$ on day 234 (Deng et al. 2004), we find the luminosity $L \approx 3.8 \times 10^{41}$ erg s $^{-1}$ which significantly exceeds the upper limit found for $S/S_0 = 1$. This means that either $S/S_0 \gg 1$ or the emission feature at

8500 Å is dominated by O I 8446 Å as Deng et al. (2004) suggest. Below we will see that the contribution of the O I 8446 Å line is small so the high luminosity of the Ca II triplet is primarily due to the large area ratio.

To show the effect of Q_0 we consider the transparent case $Q_0 = 0$ and modestly opaque shell $Q_0 = 1$ for $\tau \gg 1$. The calculated profiles for a constant velocity shell with $v_s = 6000$ km s $^{-1}$ and $\xi = 0.05$ are shown in Fig. 6 (upper panel). The finite optical depth smooths the boxy profile as expected. In the limit of $Q_0 \gg 1$, the profile is parabolic with a weak asymmetry due to relativistic effects. The relativistic effects arising from the Lorentz transformation of the frequency, wave vector and intensity are usually ignored in SN spectrum calculations. However as was demonstrated by Jeffery (1993) these effects become noticeable even for expansion velocities of $\sim 10^4$ km s $^{-1}$ and generally result in the skewing of an emission component towards blue.

3.1.3 Non-local scattering in SN ejecta

Although the contribution of the net emission from the unshocked SN ejecta is small for SN2002ic given the domination of the shock luminosity, the SN ejecta can affect the line profile via the scattering of line photon emitted by the CDS. If the SN ejecta are optically thick in the same line, then a line photon emitted by the shell inwards can scatter on the unshocked Ca II ions at the resonance point with the distance from the emission point

$$s = R|\mu| \left(1 - \frac{v_s}{v_{sn}}\right), \quad (5)$$

where $\mu = \cos \theta < 0$. The resonance points reside on a sphere of radius $(1 - v_s/v_{sn})R/2$ that contains the emitting point ($s = 0$ for $\mu = 0$).

To compute the effect of the non-local scattering of line photons in SN ejecta we adopt the boundary velocity of the SN ejecta $v_{sn} = 9000$ km s $^{-1}$; this value and the shell velocity (6000 km s $^{-1}$) are close to velocities in the standard model around day 230 (Fig. 1). Let r_c be a cut-off radius (in units of R_s) defined in such a way that the Sobolev optical depth of the SN ejecta $\tau_{sn} = 0$ in the outer zone, $r > r_c$, and $\tau_{sn} > 0$ in the inner zone, $r \leq r_c$. In both models the effect of non-local resonance scattering is shown for two cases: $r_c = 0.95$ and $r_c = 0.9$, assuming $\tau_{sn} = 5$ in the unshocked SN (Fig. 6, lower panel). Profiles demonstrate significant skewing towards the blue and the emergence of a symmetric broad base produced by scattered photons in the fast SN ejecta with velocity $v_{sn} > v_s$. The shape of the line profile depends on r_c : the skewing is larger for larger r_c . As we see below, the non-local scattering can account for the asymmetry of the Ca II doublet observed in SN 2002ic.

3.2 Models of the Ca II features

We start with the modeling of the Ca II doublet. A Monte Carlo technique is used for the radiation transfer computations. The parametrized emission rate of the CDS fragments in lines of the Ca II doublet is set assuming equipartition of the upper levels. The non-local interaction in the shell is treated as a pure absorption process, whereas the resonance interaction of line photons with the unshocked SN ejecta is

Table 1. Model parameters

| Model | Q_0 | v_s km s $^{-1}$ | v_{sn} km s $^{-1}$ | r_c | τ_{sn} | $C(\text{O I})$ |
|-------|-------|-----------------------|---------------------------------|-------|--------------------|-----------------|
| DC0 | 0 | 5936 | 9092 | 0.95 | 3 | |
| DC1 | 1 | 5936 | 9092 | 0.95 | 3 | |
| DL0 | 0 | 5936 | 9092 | 0.95 | 3 | |
| DL1 | 1 | 5936 | 9092 | 0.95 | 3 | |
| TL0 | 0 | 6053 | 9230 | 0.95 | 0.005 | 0.25 |
| TL0 | 1 | 6053 | 9230 | 0.95 | 0.005 | 0.25 |

considered as pure scattering. The quasi-continuum radiation, presumably emitted by the shell can be scattered by Ca II lines of SN ejecta, whereas the scattering in other lines (e.g., Fe II) is neglected. The quasi-continuum intensity, the slope of the emergent spectrum, and the relative line intensity are free parameters.

The calculated Ca II doublet assuming a constant velocity and an occultation optical depth $Q_0 = 0$ (model DC0) and $Q_0 = 1$ (model DC1), and assuming a linear velocity distribution with the same Q_0 values (models DL0 and DL1, respectively) are shown in Fig. 7 overplotted on the spectrum on day 244 (Wang et al. 2004). The computed spectra are smoothed by a gaussian filter with $\text{FWHM} = 7 \text{ \AA}$ to take into account the finite spectral resolution. Velocities v_s and v_{sn} of the standard interaction model as well as other parameters are presented in Table 1. The table gives also Q_0 , the optimal cut-off radius (r_c) and the optical depth of the SN ejecta in the Ca II 3934 \AA line (τ_{sn}). We found that efficient scattering in the SN ejecta is needed with $\tau_{\text{sn}} \geq 3$ in Ca II 3934 \AA . The optimal cut-off radius for all the models, $r_c = 0.95$, coincides with the inner boundary of the line-emitting shell.

All four models shown in Fig. 7 reproduce the major properties of the observed Ca II doublet, particularly, the width, shape and the skewing towards the blue. The deviation in the red wing may be related to the behavior of the underlying quasi-continuum in the observed spectrum. Models with constant and linear velocity laws in the shell are practically indistinguishable. We will use below only the linear law model that presumably mimics the possible random component of the velocity field in the shell.

Using models DL0 and DL1, we also simulated the Ca II triplet (Fig. 8). The model profiles are overplotted on the observed profile in the Subaru spectrum on day 234 (Deng et al. 2004). Parameters of the corresponding models (TL0 and TL1) including velocities of the standard model are given in Table 1 together with the optimal contribution of the O I 8446 \AA line to the 8500 \AA feature $C(\text{O I})$. The overall fit of the model TL0 is satisfactory. The derived contribution of the O I 8446 \AA line to the 8500 \AA feature $C(\text{O I}) = 0.25$ is constrained with an uncertainty of ± 0.05 . However, model TL1 with $Q_0 = 1$ shows a pronounced central absorption feature caused by the resonance non-local absorption in the shell. This feature is inconsistent with the observed profile. We conclude that the fragmented shell should be characterized by a low probability of non-local radiation coupling in the Ca II triplet. We will return to this issue below (Sec. 3.3).

The observed 8500 \AA profile is slightly broader than the

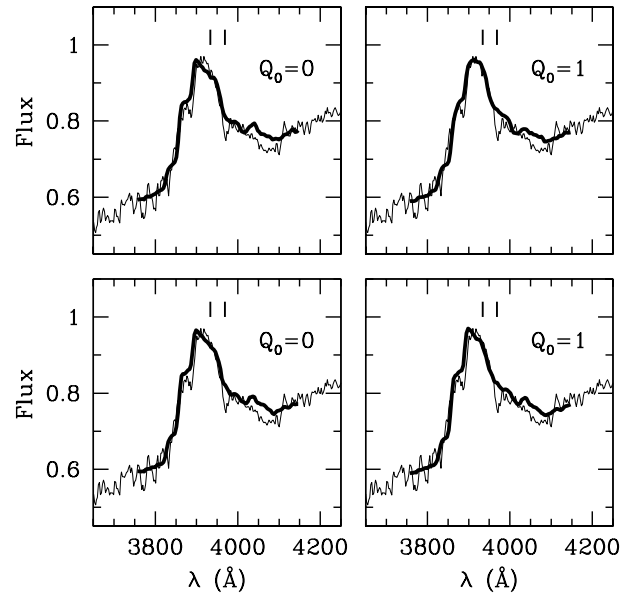


Figure 7. Calculated profiles of the Ca II 3934, 3968 \AA doublet (thick line) overplotted on the spectrum on day 244 (Wang et al. 2004). Upper panels show models with constant velocity in the shell and different Q_0 (model DC0, left, and model DC1, right). The lower panels are the same except for the linear velocity distribution in the shell (model DL0, left, and model DL1, right). Two vertical bars show the rest frame positions of 3934 \AA and 3968 \AA lines.

model feature, especially in the wings. However, one must be cautious about attributing the wings to the Ca II triplet because the quasi-continuum also contributes to the 8500 \AA feature, as will be demonstrated below. Given the uncertainties of the behavior of the quasi-continuum and the satisfactory fit of the Ca II doublet and triplet, we conclude that the Ca II features are consistent with a spherical model and expansion velocities predicted by the interaction model.

We performed computations with velocities multiplied by a factor larger than unity. We found that slightly larger expansion velocities (by $\sim 5\%$) produce better fits to the 8500 \AA features. However, this conclusion is uncertain because of a possible contribution from the quasi-continuum.

3.3 CDS temperature and S/S_0 ratio

The contribution of the O I 8446 \AA line to the 8500 \AA feature found on day 234 ($\sim 25\%$), combined with the total flux $\approx 4.7 \times 10^{-14} \text{ erg s}^{-1} \text{ cm}^{-2}$ (Deng et al. 2004), implies a flux in the O I 8446 \AA line $\approx 1.2 \times 10^{-14} \text{ erg s}^{-1} \text{ cm}^{-2}$, and $\approx 3.5 \times 10^{-14} \text{ erg s}^{-1} \text{ cm}^{-2}$ in Ca II triplet. Given the Ca II doublet flux $\approx 10^{-14} \text{ erg s}^{-1} \text{ cm}^{-2}$ in the same spectrum (Deng et al. 2004), one gets the triplet-to-doublet ratio $F(8579)/F(3945) \approx 3.5$. Assuming that both Ca II excited terms (^2D and ^2P) have the same excitation temperature and using the scaling $F \propto \nu B_\nu(T)$ from the ratio $F(8579)/F(3945) \approx 3.5$ we obtain $T \approx 4430 \text{ K}$.

The absolute luminosities of the Ca II features can be used to estimate T and the area ratio S/S_0 simultaneously

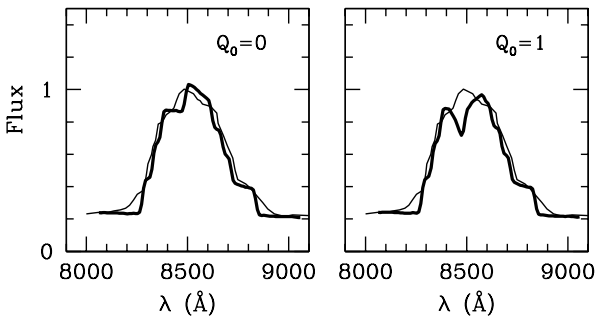


Figure 8. Calculated profile of the Ca II infrared triplet blended with O I 8446 Å for the models TL0 (left) and TL1 (right) overplotted on the observed profile on day 234 (Deng et al. 2004).

(see equation [4]). To make the procedure reliable, we abandoned the assumption that the excitation temperature for both excited terms is the same. Instead, the statistical equilibrium for a three level Ca II model is solved with collisional and radiative transitions taken into account. The radiation transfer in a fragment is treated in the static average escape probability approximation. The adopted Ca abundance is 0.03 by mass, the same as used in Section 3.1.1. The ionization fraction of Ca II is calculated in the LTE approximation, which implies that Ca II is the dominant stage for a wide range of temperature, 4000 – 6000 K. The solution of statistical equilibrium then yields the excitation temperature in both Ca II transitions as a function of the electron temperature T_e and S/S_0 , which permits us to calculate the luminosities of the Ca II features (equation [4]) and to determine T_e and S/S_0 from a comparison with the observed luminosities.

The Ca II levels are found to be well thermalized, so to reproduce the observed luminosities of Ca II features we need only two parameters: T_e and S/S_0 , assuming $\xi = 0.05$. Figure 9 shows the behavior of the luminosities of the Ca II features as a function of S/S_0 for the optimal temperature $T_e = 4430$ K. The plot clearly demonstrates that the observed luminosities of the Ca II features can only be reproduced for a large area ratio, $S/S_0 \sim 10^2$. This result provides strong evidence that the dense material of the shocked ejecta experienced substantial deformation, fragmentation and mixing in the intershock layer.

We studied the sensitivity of the luminosity of Ca II lines to the adopted mass locked in line-emitting fragments (M_e) and found that in the range of $S/S_0 < 300$ the luminosity of both Ca II multiplets are well reproduced for $M_e \geq 10^{-2} M_\odot$ and cannot be reproduced for smaller mass, $M_e < 10^{-2} M_\odot$. This indicates that the amount of the Ca-rich matter locked in the Ca II line-emitting gas is $\geq 0.01 M_\odot$ (for the mass fraction of Ca ≈ 0.03).

The conclusion that the area ratio is as large as $\sim 10^2$ raises a serious problem. The local occultation optical depth of the shell with an area ratio $S/S_0 \sim 10^2$ is $Q_0 \sim 1$. This seems inconsistent with the claim (Sec. 3.2) that the non-local radiative coupling in the Ca II triplet is weak. For the spherical shell, this requirement implies $Q_0 \ll 1$. In an attempt to resolve the inconsistency, we considered a model of

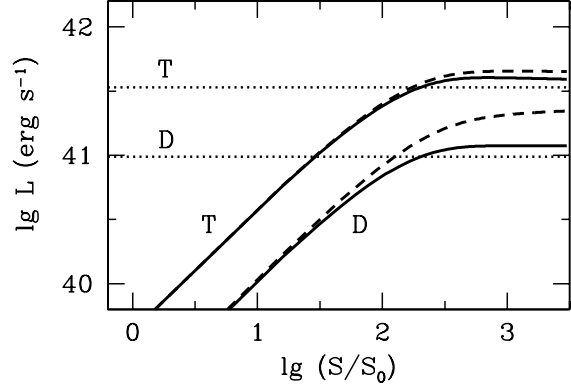


Figure 9. Calculated luminosities of the Ca II doublet and triplet on day 234 as a function of the area ratio for $T_e = 4430$ K with zero albedo (thick line) and finite albedo (dashed line) of dense fragments. The observed luminosities of the Ca II doublet and infrared triplet are plotted by dotted lines. Subscripts T and D refer to triplet and doublet feature.

the Ca II feature formation with a finite albedo ω of dense fragments for the incident line photons. To determine ω we performed a Monte-Carlo simulation of the history of the incident Ca II doublet and triplet photons assuming a three level model of Ca II. The line luminosities for the finite albedo are shown in Figure 9. The required value of the area ratio in the new model is only slightly lower compared with the previous model, so the problem of large Q_0 remains unsettled.

A way out might be in the assumption that the accepted model of the fragmented shell is too simple to predict the upper limit for the occultation optical depth from the Ca II triplet. For instance, the large scale corrugation of the shell and/or patchy structure of the line-emitting zones might result in voids lacking the absorbing dense gas at the resonance points. As a result, the large local value of Q_0 may be reconciled with the low absorption probability for the non-local interaction in the Ca II triplet.

3.4 Quasi-continuum model

We now check our conjecture that the quasi-continuum of SN 2002ic is produced by the emission of the fragmented cool shocked ejecta in numerous lines of Fe-peak elements. To this end, we compute the emergent spectrum assuming a model of the fragmented shell width $\Delta R/R = 0.1$ for two values of the area ratio $S/S_0 = 50$ and $S/S_0 = 1$. The shell patchiness indicated by the Ca II triplet modelling will be described by the surface (and volume) filling factor f_{qc} of quasi-continuum emitters. It should be emphasized that the filling factor refers only to the volume fraction of mixture and not to the volume fraction of the dense material that is, of course, much lower. The radiation transfer in the shell will be computed assuming a spherical shell, with two corrections. First, the emitting volume will be multiplied by the factor f_{qc} , and, second, we take into account a finite probability of the photon escape through the holes of the opposite side of shell, $w = |\mu|(1 - f_{qc})$. Here μ , the cosine between the photon wave vector and the radius, describes approxi-

mately the angular dependence of w . The unshocked ejecta will be considered as transparent and the net emission of this ejecta will be neglected. We also omit the presence of a shocked H-rich cool gas in the intershock layer.

We consider the seven most abundant Fe-peak elements, Ti, V, Cr, Mn, Fe, Co, Ni, assuming their relative abundance to be solar. The latter is a sensible approximation for the explosive nucleosynthesis in the full incineration regime. Doublet and triplet lines of Ca II are also included in the line list. The initial line list is extracted from the VALD data base (Kupka et al. 1999) assuming conditions in a red giant atmosphere with $T_{\text{eff}} = 5000$ K and gravitational acceleration $\log g = 1.5$. The list contains about 19000 lines of neutral and singly ionized species with a line optical depth $> 10^{-5}$ in the range of $3500 - 10000$ Å. Using this list, we compile the input line list for a particular density, assuming Saha ionization with a temperature T_{ion} and Boltzmann excitation with a temperature T_{ex} . The line optical depth is restricted by the condition $\tau > 10^{-4}$. For the relevant conditions, the most abundant species are singly ionized ($\phi_2 \approx 1$), while the ionization fraction of neutrals is $\phi_1 \sim 10^{-2}$ and that of double ions is $\phi_3 \sim 10^{-6}$.

The radiation transfer is calculated using a Monte Carlo technique. The photon interaction with a dense fragment is treated as a partial absorption with an albedo ω . We adopt $\omega = 0.1$ for all the lines, although we found that the result is practically the same in the case of pure absorption ($\omega = 0$). Scattering is assumed to be isotropic for the back and forward scattering with a diffusion reflection probability $\tau/(1 + \tau)$. The computed spectrum is reddened using $E(B - V) = 0.06$ (Deng et al. 2004).

An extensive search in the parameter space (T_{ion} , T_{ex} , f_{qc}) for the model with $S/S_0 = 50$ led us to conclude that a best fit of the quasi-continuum in the spectrum on day 244 is attained for the parameters $T_{\text{ion}} = 6000$ K, $T_{\text{ex}} = 4300$ K, and $f_{\text{qc}} = 0.125$ (Fig. 10a). Note, the result is not very much sensitive to the area ratio; we adopt $S/S_0 = 50$, not 100 that follows from Ca II line analysis, because the latter value leads to a too large occultation optical depth (see discussion in Section 3.3). On the other hand, the optimal model with the small area ratio, $S/S_0 = 1$ and $f_{\text{qc}} = 1$ (Fig. 10b) seems to be inconsistent with the observed shape of the quasi-continuum. This implies that the model with a large area ratio is preferred thus supporting the conclusion made from Ca II line analysis.

The fit is good despite the fact that the quasi-continuum model is rudimentary; the number of free parameters is small. The agreement suggests that we are on the right track in the interpretation of the quasi-continuum. This result makes the identification of [O I], [O II], [Ca II] lines for the 6400 Å and 7300 Å bumps (cf. Deng et al. 2004) unnecessary. Otherwise, there would be serious problems in the interpretation of the identified emission lines. Another remarkable fact is that the quasi-continuum contributes to the 8500 Å emission feature thus alleviating the problem of the origin of broad wings in the Ca II/O I 8500 Å feature. We checked the contribution of different ions to the quasi-continuum and found that, as expected, the Fe II lines are dominant. This elucidates the role of the ionization temperature as a fitting parameter that regulates the contribution of neutral species, Fe I in particular. The quasi-continuum in the region $\lambda < 5500$ Å is very reminiscent to that in early

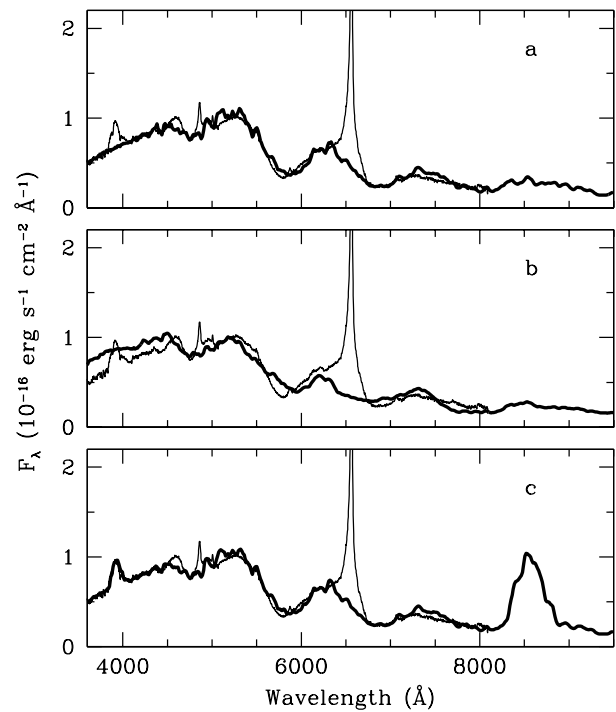


Figure 10. Synthetic spectra for the model of a fragmented shell overplotted on the observed spectrum of SN 2002ic on day 244 (Wang et al. 2004). Panel *a* shows the model with a large area ratio ($S/S_0 = 50$, see text), whereas panel *b* shows a model with $S/S_0 = 1$. Panel *c* shows the same model as in panel *a* but with the addition of a Ca II line-emitting zone.

SN 1988Z, which also has been identified with Fe II lines (Chugai & Danziger 1994).

Interestingly, the smooth quasi-continuum in the range $\lambda < 4500$ Å (Fig. 10a) is the result of radiation saturation at the Planck intensity due to the high density of lines in this band that results in the large optical depth of the shell, viz. $\tau_{\text{shell}} \sim \langle Q \rangle N_{\text{line}} > 1$, where N_{line} is the number of lines in the characteristic wavelength interval $\lambda(v_s/c)(\Delta R/R)$ with the average local occultation optical depth $\langle Q \rangle$. The saturation effect is absent in a model with small area ratio $S/S_0 \sim 1$ (Fig. 10b). Because the line density in the ultraviolet (UV) region is very high, we expect that the UV quasi-continuum should retain a smooth black-body appearance with $T \sim 4300$ K in the short wavelength region ($\lambda < 3500$ Å).

As shown in Fig. 10a, the quasi-continuum model is unable to produce strong Ca II emission features. This is related to the fact that the quasi-continuum is a superposition of a large number of weak lines affected additionally by the line overlapping. We propose, therefore, that the Ca II emission and quasi-continuum should form in *different* zones of the shocked ejecta. These zones, presumably, correspond to Fe-poor (Ca-rich) gas and Fe-rich gas, respectively. The obvious physical reason for these distinctive zones is the abundance stratification of SNe Ia with the inner layers incinerated up to Fe-peak elements and the outer layers having undergone incomplete burning. In this situation one expects that the outer Fe-poor gas that has passed through the re-

verse shock first has enough time to spread over the large volume of the intershock layer, whereas the inner Fe-rich material shocked recently occupies only a small fraction of the intershock layer.

To illustrate the proposed scenario for the Ca II lines, we consider a combined model of the fragmented shell: apart from the quasi-continuum line-emitting zones suggested by the model with $f_{qc} = 0.125$, we consider the Ca II line-emitting zones with a filling factor $C(1 - f_{qc})$, where C is a fitting parameter. We assume a Ca abundance ≈ 0.03 by mass (the result only weakly sensitive to Ca abundance) and neglect the Fe-peak elements in the Ca II line-emitting zone. For Ca II lines, the scattering in the unshocked SN ejecta on Ca II is taken into account as described in the previous section. The same area ratio $S/S_0 = 50$ and $T_{ex} = 4300$ K are adopted in the Ca II and quasi-continuum zones. We omit here the contribution of O I 8446 Å.

The result presented in Fig. 10c is obtained for $C = 0.8$, which suggests that $\sim 70\%$ of the fragmented shell volume is occupied by Fe-poor Ca II line-emitting material. The filling factor again refers only to the volume fraction of the mixture and not the dense material. Although we do not intend to describe the Ca II profiles and intensities in detail, the combined model provides a satisfactory representation of the overall spectrum, except for H α and H β . The modelling thus confirms the proposed scenario based upon the expected abundance stratification in the outer layers of the SN ejecta.

We now address the question of how low the abundance of Fe-peak elements in the Ca II line-emitting matter can be and retain sufficient contrast between the quasi-continuum and the Ca II lines, especially the Ca II doublet that resides in the line-rich spectral range. The answer depends on the assumed mass locked in the Ca II line-emitting dense gas (M_e). We adopt $M_e \approx 0.02 M_\odot$ and a Ca abundance 0.03, which is close to the admissible lower limit ($M_e \geq 0.02 M_\odot$) and is consistent with the mass and composition of the Fe-poor Ca-rich layer produced by the delayed detonation model (Iwamoto et al. 1999). For these parameters and the values of T_{ion} and T_{ex} adopted above for the case of $S/S_0 = 50$, we found that the mass fraction of Fe-peak elements should not exceed 2×10^{-4} or ~ 0.1 of solar abundance. This upper limit indicates a low primordial metallicity of the pre-SN and, possibly, of the host galaxy as well.

To summarize, the major observational properties of the SN 2002ic spectrum at an age of ~ 240 days may be explained in the framework of a model of a spherical, locally inhomogeneous shell with an expansion velocity predicted by the standard hydrodynamic model.

4 DISCUSSION AND CONCLUSIONS

The aim of this paper was to develop a unified model for the light curve and spectrum of SN 2002ic assuming approximate spherical symmetry. Our principal result is that the Ca II line profiles and the quasi-continuum are consistent with the interaction model provided that the SN Ia has the maximum possible kinetic energy.

The high explosion energy is in line with the high peak absolute magnitude of SN 2002ic. According to Hamuy et

al. (2003), at light maximum SN 2002ic was as bright as $M(V) \approx -20.3$ ($H_0 = 65 \text{ km s}^{-1} \text{ Mpc}^{-1}$). Given the contribution of the veiling continuum of about 0.3 mag on Dec. 3 in V band (5000 – 6000 Å) (Hamuy et al. 2003), we conclude that the peak absolute magnitude of the SN Ia was $M(V) \approx -20$, close to that of extremely bright SN Ia, SN 1991T ($M(V) \approx -20.2$, cf. Fisher et al. 1999). The magnitude at the maximum coincides also with that predicted by the detonation model DET1 (Höflich & Khokhlov 1996). This coincidence is another justification for our choice of the high kinetic energy for the SN 2002ic event. Yet, as we noted above, the strong Ca II emission lines indicate that the explosion should be different from the DET1 model in the sense that the degree of incineration in the outer layers should be lower to produce enough ($\geq 10^{-2} M_\odot$) Ca-rich Fe-poor material.

Modeling of the spectra of the fragmented cool dense shell formed in the intershock layer provides strong evidence that the quasi-continuum and Ca II lines are emitted by different zones. This presumably reflects the stratification of the composition of the SN ejecta in the sense that the outer layers responsible for the Ca II lines are Fe-poor, while the inner layers responsible for the quasi-continuum are Fe-rich. The Fe-poor ejecta are shocked earlier and, therefore, spread throughout the intershock layer, while Fe-rich ejecta are shocked later and thus have not yet mixed with the Fe-poor material at $t \sim 240$ d. This picture predicts that at a later epoch ($t > 240$ d) both Fe-poor and Fe-rich shocked components should be mixed with each other. As a result, the Ca II doublet must disappear at a later epoch due to the mixing of the Ca II line-emitting gas with optically thick quasi-continuum emitters. SN 1999E showed a gradual disappearance of the Ca II 3945 Å doublet in spectra between days 139 and 361 (Rigou et al. 2003), in accord with these expectations.

The high luminosity of the Ca II doublet and triplet in SN 2002ic on day 234 indicates that the dense shocked ejecta form a structure with a large area ratio, $S/S_0 \sim 10^2$. A high area ratio ($S/S_0 \sim 50$) is also preferred by the quasi-continuum model. The area ratio, which is common in the treatment of the physics of mixing fluids (e.g., Catrakis et al. 2002), has not been used before in the interpretation of optically thick emission lines from an intershock layer. It was recognized earlier that the interpretation of the X-ray and radio emission of an interacting SN depends on the presence of a mixing layer, while the H α emitted by the mixed dense material may reveal the fine structure related to the RT spikes (Chevalier & Blondin 1995). Here we add to the list of effects of the mixing layer the crucial role of the large area ratio for the interpretation of the Ca II lines and quasi-continuum in SN 2002ic.

The fact that the area ratio in SN 2002ic on day 234 is large, $S/S_0 \sim 10^2$, suggests that we observe an advanced stage of the mixing of dense shocked ejecta in the intershock zone. Experiments on the mixing of fluids show that the interface between fluids reveals fractal behavior. Specifically, the cumulative area of the interface above the scale λ is $S \propto \lambda^{-\alpha}$, where $\alpha \approx 0.35$ (Sreenivasan et al. 1989). If this law also holds in the case of the mixing of the dense shocked ejecta in the intershock layer of SN 2002ic, then the dense gas should produce structures with scales as small as $\lambda/R \propto (S/S_0)^{-1/\alpha} \sim 10^{-6}$. The minimum linear scale that

corresponds to the thickness of the dense fragments should be even smaller, $\sim \delta(S_0/S) \sim 10^{-8} R$, where δ is the original thickness of the CDS (Section 3.1). It would be interesting to check the possibility of creating the mixing layer in SN 2002ic with $S/S_0 \sim 10^2$ in numerical experiments using high resolution 3D hydrodynamical simulations, although it seems to be beyond the capabilities of present-day computers. To estimate the area ratio from a numerical experiment, one needs to find the average number of intersections of dense peaks with the radius in the intershock layer N_{is} . The area ratio is then $S/S_0 \approx 2N_{\text{is}}$.

We do not yet fully understand all the mechanisms responsible for the major spectral features seen in the late emission from SN 2002ic. In addition to the $\text{H}\alpha$ line, an important issue ignored in our study is the problem of the O I 8446 Å emission, although it is not a dominant constituent of the 8500 Å bump anymore. The oxygen excitation mechanism should predict the absence of strong O I 7774 Å in SN 2002ic. The fluorescence pumping of O I 8446 Å in the $\text{H}\alpha$ -emitting gas (Deng et al. 2004) meets this requirement. This mechanism predicts a comparable intensity of O I 11287 Å. The absence of this line in the spectrum of SN 1999E around ~ 200 d (Rigon et al. 2003, their Fig. 6) casts doubt on the fluorescence mechanism. An alternative possibility is that the O I 8446 Å line is emitted by the oxygen-rich matter in the outermost layers of the SN ejecta due to non-thermal collisional excitation by secondary electrons that are created by high energy photoelectrons. Excitation by secondary electrons also yields a high O I 8446 Å/ O I 7774 Å intensity ratio (Stolarski & Green 1967). An interesting possibility that $\text{Ly}\alpha$ pumping line of Fe II 8451 Å might contribute to 8500 Å band instead of O I 8446 Å, as was the case, possibly, for SN 1995N (Fransson et al. 2000), seems unlikely here because of the absence of another strong $\text{Ly}\alpha$ fluorescent band of Fe II at ~ 9150 Å. Despite of a possible presence of a large amount of oxygen in the cool shocked SN gas (up to $\sim 0.1 M_\odot$), the strong $[\text{O I}]$ line is not expected. Adopting Boltzmann population for $T = 4400$ K and oxygen mass of $0.1 M_\odot$ one gets the luminosity of this line of about $\sim 10^{39}$ erg s $^{-1}$, i.e., a factor of $\sim 10^{-2}$ lower compared to the luminosity of the observed "6300 Å" emission band on day 244.

In view of the possibility that our hydrodynamic model may underestimate the expansion velocity of the SN/CSM interface by about 5%, we discuss the implications for our model. The emergent X-ray luminosity from the forward shock in the standard model is comparable or even exceeds the optical bolometric luminosity after maximum light (see Fig. 1 and Fig. 3). Hence, there is an extra energy reservoir which might, in principle, be transformed into the optical band under the proper conditions. This possibility could be realized in a model of interaction with a clumpy CSM. As a result of (i) softer X-rays from cloud shocks than for a smooth CSM, and (ii) the larger geometrical probability of absorption of X-rays from clouds penetrating the SN ejecta, the optical output from the interaction should be larger. Therefore, the same bolometric luminosity can be produced for a lower average CS density and higher expansion velocity of the SN/CSM interface compared with a smooth CSM.

The spherical geometry of the CS interaction of SN 2002ic, advocated here, finds additional support from statistical arguments already mentioned in the Introduction.

We know three events of SNe Ia in a dense CSM (SN 1997cy, SN 1999E, SN 2002ic) and they show similar widths and shapes of spectral features at a similar phase (see Deng et al. 2004, their Fig. 1). This fact suggests that a bi-polar structure of the SN/CSM interface with high aspect ratio is unlikely.

At first glance the picture of spherical interaction is incompatible with the detection of intrinsic polarization of SN 2002ic radiation at a level of $\sim 0.8\%$ (Wang et al. 2004). Simple estimates show that the Thomson scattering in a moderately aspherical CS envelope with $\tau_T \approx 0.1$ is not able to produce such a high polarization. The issue may be resolved in a model in which the polarization is acquired in the scattering of the SN radiation on the dust in a distant ($\geq 10^{17}$ cm) aspherical CSM.

The resemblance of the light curves for all three SN 2002ic-like events (see Deng et al. 2004) suggests a similar regime of mass-loss from their presupernovae and a common origin of the progenitors. As mentioned before (Chugai & Yungelson 2004), the uniformity lends support for the SN 1.5 evolutionary scenario suggested by Iben & Renzini (1983). Yet we do not rule out the binary scenario. In this case, the WD companion should be a supergiant with the mass $> 2 M_\odot$ (the CS envelope, $\approx 1.6 M_\odot$, plus the supergiant core, $> 0.5 M_\odot$). In the binary scenario, there is no clear reason for the supergiant to have experienced strong mass loss just before the SN explosion. The synchronization of the vigorous mass loss and the SN event might be a more natural outcome in the single AGB star scenario with the C/O core approaching the Chandrasekhar limit.

A general belief is that Chandrasekhar mass white dwarfs cannot be produced from intermediate-mass single stars because the growth of the C/O core during the thermal pulsation stage is prevented by the removal of the hydrogen envelope (Blöcker 1995, and references therein). In this regard, it is highly remarkable that at least two supernovae (SN 2002ic and SN 1997cy) exploded in dwarf galaxies, as already noted by Chugai & Yungelson (2004). Dwarf galaxies are characterized by low metallicity, which thus might explain why the CO core of an asymptotic giant branch star is successful in attaining the Chandrasekhar limit before the hydrogen envelope is lost (Chugai & Yungelson 2004). An evidence for the low metallicity of the presupernova of SN 2002ic comes from our modelling of the Ca II lines and quasi-continuum (Sec. 3.4). The possibility of SN 1.5 explosions in metal-poor galaxies was suggested also by Zijlstra (2004). It would be interesting to check whether all the host galaxies of SN 2002ic-like supernovae are actually metal deficient. If the suggested link between SN 2002ic-like events and low metallicity is correct, then their occurrence rate relative to normal SN Ia must increase with the redshift for $z > 2 - 3$, when the average cosmic metallicity was lower than solar.

If SN 2002ic-like events stem from SN 1.5 explosions, their low fraction of SN Ia, $< 1\%$, can be used to estimate the fraction of white dwarfs created with a mass similar to the Chandrasekhar mass. If only $\sim 1\%$ of all WDs can become SN Ia, this suggests that only $\lesssim 10^{-4}$ of white dwarfs in our Galaxy were formed with a mass close to the Chandrasekhar mass. Since these white dwarfs are likely to have formed in a metal poor environment, they are probably very old (age $\sim 10^{10}$ yr) and thus of low luminosity,

$< 3 \times 10^{-5} L_\odot$ (Prada Moroni & Straniero 2003). The number of known cool white dwarfs is low, < 40 (Salim et al. 2004), and will probably remain too low for the nearest future to test the idea whether high mass white dwarfs were produced during early epochs when the metallicity was low.

The possible link between SN 2002ic-like supernovae and hypothetical SN 1.5 events, combined with arguments in favour of a high energy SN Ia event in this case, raises the question of whether conditions in a hot Chandrasekhar mass C/O WD that just got rid of the remnants of the hydrogen envelope favour a WD explosion with a high kinetic energy of ejecta.

The SN 1.5 origin of SN 2002ic suggests that the initial mass at the main sequence is $\sim 8 M_\odot$. With the Chandrasekhar core and $1.6 M_\odot$ in the dense CS envelope we expect that about $5 M_\odot$ had to be lost at the previous AGB stage. This means that outside the dense CS envelope ($r > 3 \times 10^{16}$ cm) there should be a dense red supergiant wind with a velocity of the order $\sim 10 \text{ km s}^{-1}$ and a mass loss rate of $\sim 10^{-4} M_\odot \text{ yr}^{-1}$. Keeping in mind the analogy with SN 1979C, this wind may be revealed in the infrared (IR) as an IR echo (Dwek 1983), and in the radio as a result of CS interaction (Chevalier 1982a, Weiler et al. 1986). However, the radio emission from the distant SN 2002ic (~ 285 Mpc) may pose a difficult challenge to detect. If the radio luminosity is comparable to that of SN 1979C (Weiler et al. 1986) then the expected radio flux from SN 2002ic around 1000 day should be of the order of $\sim 0.03 \text{ mJy}$ in the $6 - 20$ cm band, which is close to the detection limit of VLA. A more promising target for the detection of the late time interaction of SN 2002ic-like supernovae with the presumed AGB wind is SN 1999E at a distance of ~ 112 Mpc, or any closer SN 2002ic-like event that will be discovered in the future. Note, that at the epoch of the interaction with the dense CS shell ($t < 500$ d), the radio emission is severely attenuated by free-free absorption at wavelengths $\lambda > 1$ cm. With the parameters used in our models, and adopting temperatures for the shell and wind in accordance with the models of Lundqvist & Fransson (1988), we find that free-free absorption is a likely reason why the observations of Berger & Soderberg (2003) and Stockdale et al. (2003) did not detect radio emission from SN 2002ic.

A better understanding of the phenomenon of SN 2002ic-like events requires an accurate energy audit, for which the direct detection of the X-ray emission as well as IR measurements are important. SN 2002ic-like events at an age of $200 - 500$ days are excellent targets for Chandra, XMM and INTEGRAL.

5 ACKNOWLEDGEMENTS

We are grateful to Lifen Wang for sharing his spectrum of SN 2002ic and Tanya Ryabchikova for the help in retrieving the line list from VALD. NNC received partial support from RFBR grant 02-17255 and RAC from NSF grant AST-0307366. Support from the Royal Swedish Academy is also acknowledged. PL is further supported by the Swedish Research Council.

REFERENCES

Arnett W.D., 1980, ApJ, 237, 541
 Blöcker T., 1995, A&A, 297, 727
 Berger T., Soderberg A.M., 2003, IAUC No. 8157
 Blondin J.M. 2001, in S.S. Holt and U. Hwang eds. Young Supernova Remnants. Eleventh Astrophysics Conf., AIP, p.59
 Blondin J.M., Marks B.S., 1996, NewA, 1, 235
 Blondin J.M., Ellison D.C. 2001, ApJ, 560, 244
 Catrakis H.J., Aguirre R.C., Ruiz-Plancarte J. 2002, J. Fluid. Mech., 462, 245
 Chevalier R.A., 1982a, ApJ, 258, 790
 Chevalier R.A., 1982b, ApJ, 259, 302
 Chevalier R.A., Blondin J.M., 1995, ApJ, 444, 312
 Chevalier, R.A., Fransson, C., 1994, ApJ, 420, 268
 Chugai N.N., 1992, Sov. Astron., 36, 63
 Chugai N.N., Danziger I.J., 1994, MNRAS, 268, 173
 Chugai N.N. 2001, MNRAS, 326, 1448
 Chugai N.N., Yungelson L.R., 2004, Astron. Lett. 30, 65
 Cid Fernandes R.C., Terlevich R., 1994, in Tenorio-Tagle G. ed. Violent Star Formation. From S Doradus to QSO. CUP, Cambridge, p. 365
 Deng J., Kawabata K.S., Ohyama Y., Nomoto K., Mazzali P.A., Wang L., Jeffery D.J., Iye M., 2004, ApJ, 605, L37
 Dwarkadas V.V., Chevalier R.A., 1998, ApJ, 497, 807
 Dwek E., 1983, ApJ, 274, 175
 Fisher A., Branch D., Hatano K., Baron E., 1999, MNRAS, 304, 67
 Fransson C. et al., 2002, ApJ, 572, 350
 Gerasimovič B.P., 1933, Zeitschrift Astrophys., 7, 23
 Hamuy M. et al., 2003, Nature, 424, 651
 Hueckstaedt R.M., 2003, NewA, 8, 295
 Höflich P., Khokhlov A.M., 1996, ApJ, 457, 500
 Iben I. Jr., Renzini A., 1983, Annual Rev. Astron. Astrophys. 21, 271
 Itikawa Y., Ichimura A., 1990, J. Phys. Chem. Ref. Data, 19, 637
 Iwamoto K., Brachwitz F., Nomoto K., Kishimoto N., Umeda H., Hix W.R., Thielemann F.-K., 1999, ApJS, 125, 439
 Jeffery D.J., 1993, ApJ, 415, 734
 Khokhlov A.M., Müller E., Höflich P., 1993, A&A, 270, 223
 Kupka F., Piskunov N., Ryabchikova T.A., Stempels H.C. & Weiss W.W., 1999, A&AS, 138, 119
 Livio M., Riess A., 2003, ApJL, 594, L93
 Lundqvist P., Fransson C. 1988, A&A, 192, 221
 Madej J., Należyty N., Althaus L.G., 2004, A&A, 419, L5
 Prada Moroni P.G., Straniero O., 2003, Mem.S.A.It., 74, 508
 Rigon L. et al., 2003, MNRAS, 340, 191
 Salim S., Rich R.M., Hansen B.M., Koopmans L.V.E., Oppenheimer B.R., Blandford R.D., 2004, ApJ, 6001, 1075
 Sreenivasan K.R., Ramshankar R., Meneveau C., 1989, Proc. R. Soc. Lond. A 421, 79
 Stockdale J., Sramek R.A., Weiler, K.W., Van Dyk, S.D., Panagia, N., 2003, IAUC No. 8157
 Stolarski R.S., Green A.E.S., 1967, JGR, 72, 3967
 Turatto M. et al., 2000, ApJL, 534, L57
 Wang L., Baade D., Höflich P., Wheeler J.C., Kawabata K., Nomoto K., 2004, ApJ, 604, L53
 Whelan J., Iben I. Jr., 1973, ApJ, 186, 1007
 Weiler K.W., Sramek R.A., Panagia N., van der Hulst J.M., Salvati M., 1986, ApJ, 301, 790
 Wood-Vasey, W. M., et al., 2002, IAUC No. 8019, 2
 Zijlstra A.A., 2004, MNRAS, 348, L23